International Journal of Thermal Sciences 198 (2024) 108874

Contents lists available at ScienceDirect

International Journal of Thermal Sciences

journal homepage: www.elsevier.com/locate/ijts

Pulsating nanofluid-jet impingement cooling and its hydrodynamic effects on heat transfer

Emmanuel O. Atofarati [a], Mohsen Sharifpur [a,b,*], Josua P. Meyer [a,c]

[a] Department of Mechanical and Aeronautical Engineering, University of Pretoria, Pretoria, Private Bag X20, Hatfield, 0028, South Africa
[b] Medical Research Department, China Medical University Hospital, China Medical University, Taichung, Taiwan
[c] Department of Mechanical and Mechatronic Engineering, Stellenbosch University, Stellenbosch, South Africa

ARTICLE INFO

Keywords:
Pulsating jet impingement
Heat transfer
Hybrid nanofluids
Hydrodynamic effects

ABSTRACT

Unlocking optimum heat transfer is essential for enhancing solar thermal collector efficiency and advancing sustainable energy solutions. This experimental study investigates a simulated solar thermal collector's heat transfer behavior using jet impingement cooling, emphasizing hydrodynamic effects in pulsating nanofluid-jet impingement. Al_2O_3-MWCNT/water hybrid nanofluid is utilized, varying pulsating frequency ($0.2\ Hz \leq F \leq 20\ Hz$), amplitude ($4\ Vp \leq A \leq 20\ Vp$), waveform (sine, squared, triangular), wave offset ($0 \leq \eth \leq 4$), and nanofluid volume fraction ($0.05\ vol\% \leq \varphi \leq 0.3\ vol\%$) to optimize heat transfer. Results show a significant influence on heat transfer performance for all parameters except waveform. A peak heat transfer enhancement of 24 % is observed for 0.3 vol% Al_2O_3-MWCNT/water compared to de-ionized water under continuous jet impingement. Additionally, a 20 % enhancement is achieved with a sine waveform at $\varphi = 0.3$ vol%, $F = 0.2$, $A = 8$, and $\eth = 2$. Pulsating jet impingement generally yields higher cooling rates, as the cooling curves indicate. These findings provide crucial insights for optimizing heat transfer in solar thermal collectors through pulsating hybrid nanofluid jet impingement cooling.

1. Introduction

Solar energy has been proven to be the cleanest, largest, and most inexhaustible source of thermal energy available to man to date. However, the challenge of harvesting this energy remains the limiting factor to its maximum utilization. However, due to its enormous heat and mass transfer rate from hot spots, Jet impingement cooling has gained significant attention from researchers and industries. Since the 1990s, several experimental, numerical and analytical studies have been carried out on jet impingement using air or liquids for cooling or heating flat [1], curved [2], smooth, rough [3], ribbed [4], micro-channeled [5], fixed or moving target bodies [6]. Many of these studies have been targeted at solving industrial problems in electronics and microchips [7], aircraft turbine blades [8], I.C. engines [9], metallurgy [10], solar thermal systems [11,12] etc. Impingement cooling could either be in the continuous or non-continuous (swirling, reciprocating, or pulsating) jet.

Most studies have proved that non-continuous jets have better heat transfer efficiency than continuous jets [13,14]. However, some other studies have shown that pulsating jet had an insignificant impact on heat transfer efficiency for the pulsating parameter range they considered [15,16]. Zhang et al. [17], while investigating the impact of pulsating jet on the heat transfer performance. They reported an improvement of 30 % and 50 % for low and high pulsating jet frequency, respectively, using air and a diaphragm solenoid considering flow Reynolds number ($2800 < Re < 10000$) and pulsating jet frequency ($0.1\ Hz < F < 2\ Hz$). They also added that the pulsating amplitude or intensity is proportional to the heat transfer enhancement at the wall region.

In another study by Trávníček et al. [14], a heat transfer improvement of 18 % was observed for the hybrid pulsating/synthetic jet, which uses a fluid diode compared to a conventional synthetic jet. Mladin & Zumbrunen [13] also reported enhanced heat transfer for pulsating jets generated with a variable speed motor and ball valve system. In most studies on pulsating jet cooling, improved heat transfer has been attributed to the continuous renewal of the hydrodynamics and thermal boundary conditions. However, Wassenberg et al. [18] explained that contra-wise, enhanced splattering, which could result from a high jet-to-target gap, leads to lower heat transfer enhancement at a higher Reynolds number.

The advent of nanofluids has also advanced jet impingement applications, as studies are now carried out to investigate the impact of these

* Corresponding author. Department of Mechanical and Aeronautical Engineering, University of Pretoria, Pretoria, Private Bag X20, Hatfield, 0028, South Africa.
E-mail address: mohsen.sharifpur@up.ac.za (M. Sharifpur).

https://doi.org/10.1016/j.ijthermalsci.2023.108874
Received 10 September 2023; Received in revised form 3 December 2023; Accepted 26 December 2023
Available online 13 January 2024

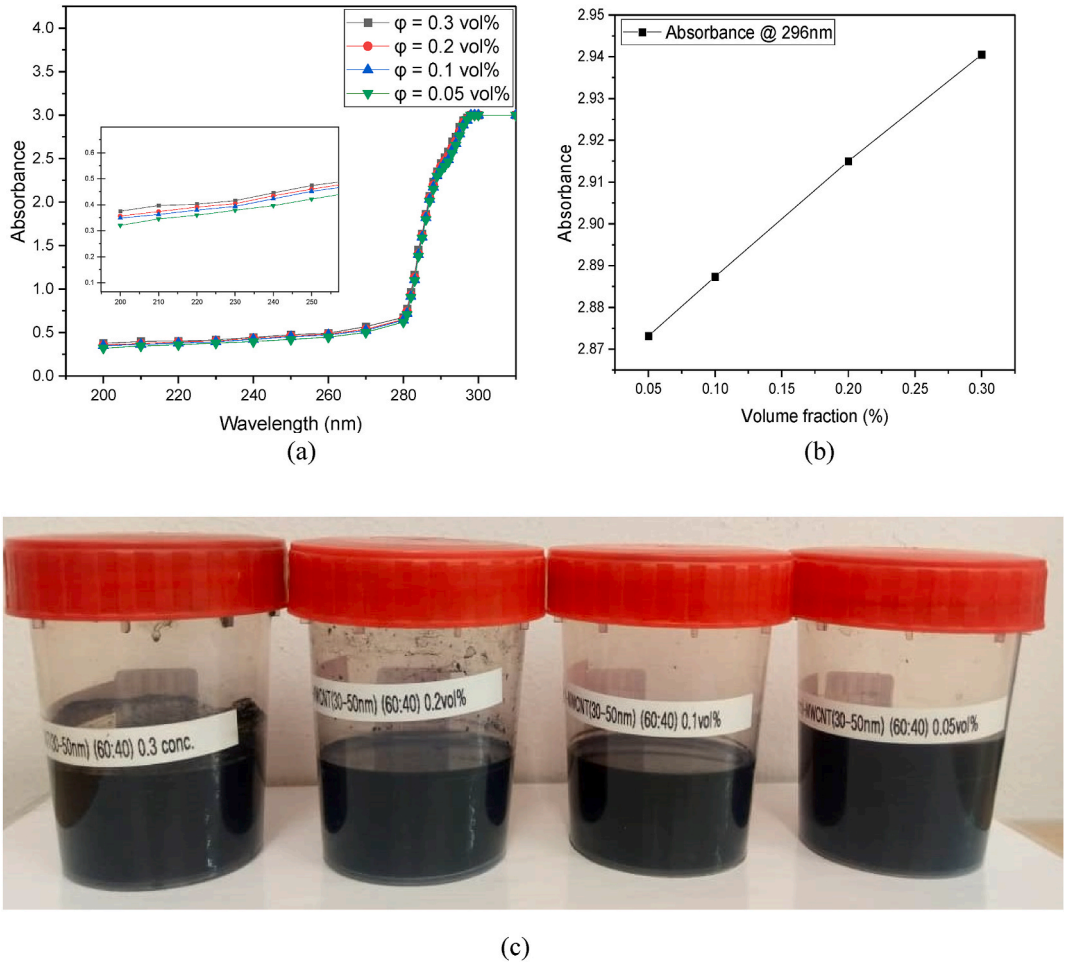

Fig. 1. Stability check for the synthesised hybrid nanofluids.

high conductivity fluids on thermal dissipation. Several works have been done on using single and hybrid nanofluids for jet impingement cooling applications as heat transfer fluid. This observation is substantiated through Sarkar et al.'s research [19], which involved an investigation into the impingement cooling performance of Cu-AL LDH nanofluid on a hot steel surface. The results revealed an impressively high cooling rate of approximately 150 °C per second. Similar enhancements in heat transfer were documented in the study by Wen et al. [20], where a notable peak thermal augmentation of 13.2 % was achieved.

In recent times, numerous numerical studies have explored pulsating nanofluid jet impingement cooling, consistently revealing its superior heat transfer performance over continuous jet cooling under various pulsation conditions. Maatoug et al. [11], conducted a numerical investigation, considering single and hybrid water-based nanofluids, and assessed the impact of pulsating amplitude, frequency, nanofluid volume fraction, and the number of impinging slots. Their findings showed that the highest amplitude at low frequency led to the most effective pulsating jet cooling with a remarkable 63.5 % enhancement. Pulsating frequency exhibited negligible influence on heat transfer performance compared to amplitude, with improved heat transfer of 22.9 %, 22.8 %, and 3.5 % for hybrid, cylindrical, and spherical nanofluids, respectively, at the highest volume fraction considered. This result is in good agreement with the findings of Selimefendigil & Oztop [21]. In their studies on synthetic and continuous single and multiple nanofluid jet impingement cooling of microchannel heat sinks, similar results were observed by Lau et al. [22] and Mohammadpour et al. [23]. Although the latter highlighted the importance of higher frequency for enhanced heat transfer, it aligns with the outcomes of Maatoug et al.

However, to the best knowledge of this author, minor or no experimental studies are available on pulsating hybrid nanofluid jet cooling using γ-Al_2O_3-MWCNT/water as heat transfer fluid for solar thermal collection. Hence, this novel experimental study is needed on pulsating nanofluid-jet impingement cooling.

This study investigates the hydrodynamic effect of pulsating frequency (0.2 Hz ≤ F ≤ 20 Hz), amplitude (4 ≤ A ≤ 20), waveform (sine, squared and triangular), wave offset (0 ≤ $\bar{\sigma}$ ≤ 4) and nanofluid volume fraction (0.05 vol% ≤ φ ≤ 0.3 vol%) on the heat transfer efficiency of (γ-Al_2O_3-MWCNT/water) hybrid nanofluids jet impingement cooling.

2. Experimental method

2.1. Nanofluids materials and preparation

The nanofluids (γ-Al2O3-MWCNT and water) were prepared through a two-step technique. In this process, the nanoparticles were dissolved in De-ionized water, resulting in the desired volume fractions (0 vol% ≤ φ ≤ 0.3 vol%). The γ-Alumina oxide (Al_2O_3) nanoparticles and Multi-Walled Carbon Nanotubes (MWCNT) were mixed in a 60:40 ratio. To prevent agglomeration, 0.5 vol% of Sodium Dodecyl Benzene Sulfonate (SDBS). The mixture was stirred for 30 min using a magnetic stirrer at a fixed speed. Subsequently, ultrasonication was performed for 1 h using a Qsonica (Q-700) sonicator at a sonication amplitude control of 90 %, within a constant temperature bath set to 20 °C. The nanofluid's physical observation and stability monitoring were carried out for 24 h using a UV-spectrophotometer, confirming its stability. Fig. 1 (a) & (b) shows the relationship between the nanofluid volume fraction, wavelength and

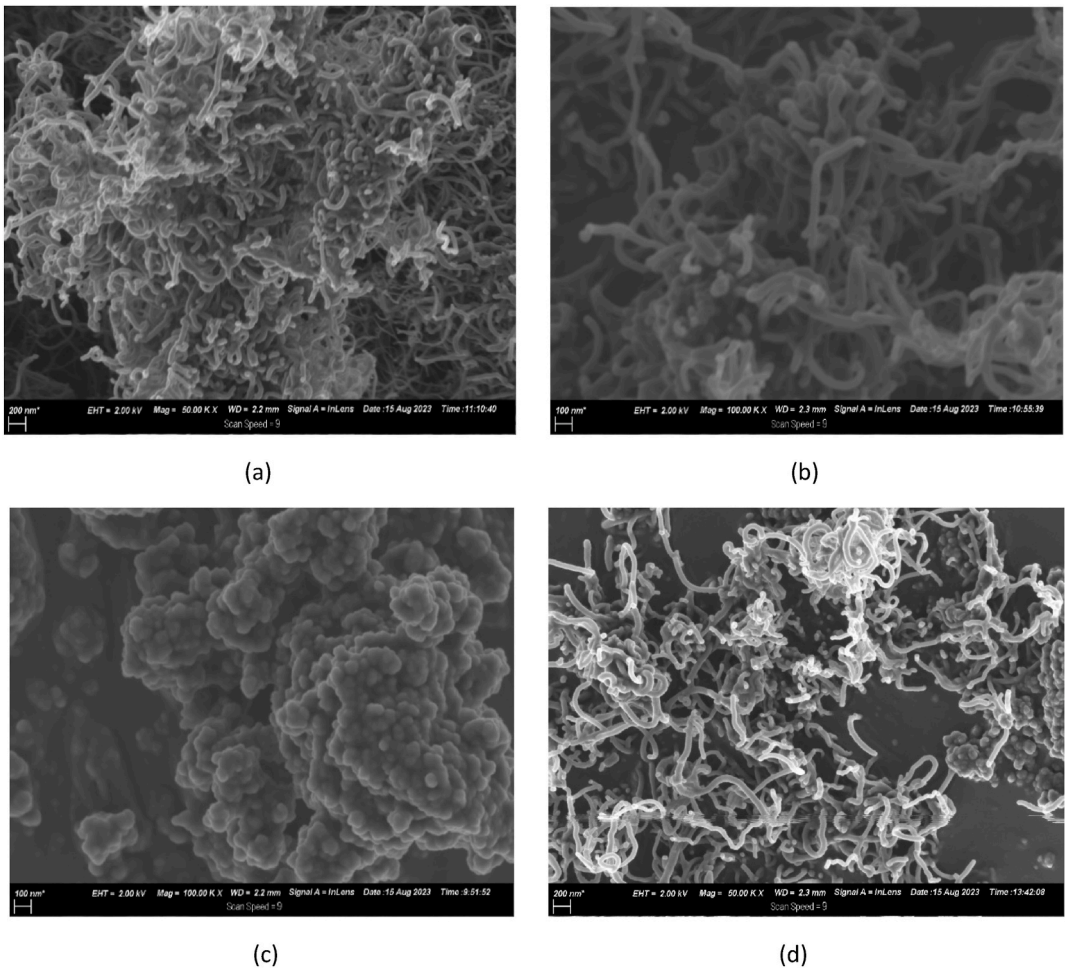

Fig. 2. FEG-SEM images of (a) MWCNT (Mag = 50 KX), (b) MWCNT (Mag = 100 KX) (c) Al2O3 (Mag = 100 KX) (c) Al2O3- MWCNT (Mag = 50 KX).

absorbance. The plot shows that absorbance was directly proportional to the volume fraction of the nanofluid, which is in good agreement with the Beer-Lambert law. Fig. 1 (c) shows the visual observation of the different volume fractions of the nanofluid after about three months.

2.2. Morphology of the nanoparticle

The examination of the morphology of γ-Al2O3 and MWCNT nanoparticles, as well as their hybrid, is depicted in Fig. 2. This comprehensive study was meticulously conducted using a Zeiss Crossbeam 540 scan field emission gun electron microscope (FEG-SEM), accessible at the Microscopy Department of the University of Pretoria. To ensure precise and detailed observations, the nanoparticle samples were thoroughly prepared before their visualization in the FEG-SEM. The morphology assessment of the γ-Al2O3 nanoparticles revealed a spherical shape with cloud-like agglomerates of particles, while the MWCNT exhibited a tubular configuration. These observed morphologies align with those reported in prior literature studies on nanoparticles, corroborating their accurate nomenclature.

2.3. Thermophysical properties measurement

2.3.1. Thermal conductivity

The thermal conductivity of the hybrid nanofluids was measured and compared to DI-water for a temperature range of 10 °C and 30 °C. The nanofluids' thermal conductivity (TC) was measured using a KD2-Pro thermal analysing meter by Decagon Devices, USA, with ±10 % accuracy. The TC meter was calibrated before measurement using the

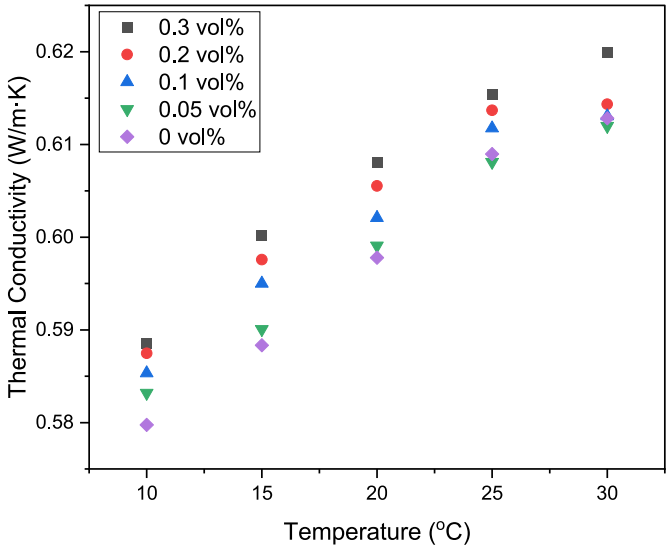

Fig. 3. Thermal conductivity of the nanofluids over a temperature range.

standard thermal conductivity fluid (Glycerine). The TC readings concerning temperature change are presented in Fig. 3 for the various nanofluid volume fractions. De-ionized water is considered as 0 vol%. The TC result shows that thermal conductivity increases with temperature and volume fraction of the γ-Al2O3-MWCNT/water nanofluid,

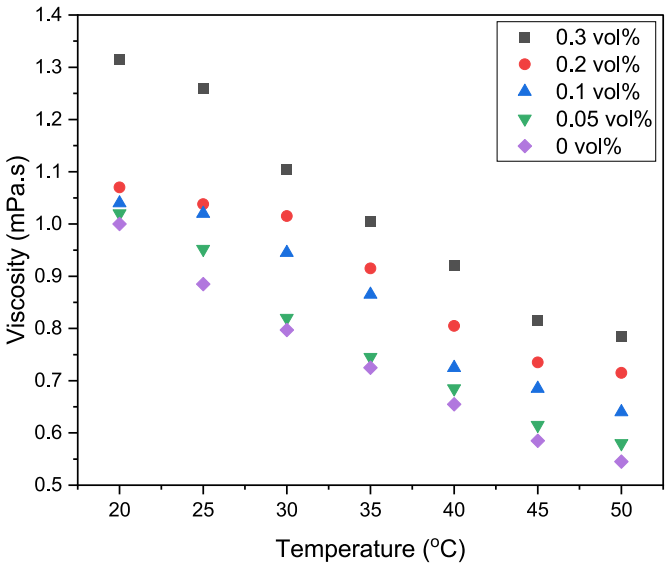

Fig. 4. Viscosity of the nanofluids over a temperature range.

which corresponds with recent work by Krishnan et al. [24] using the same hybrid nanofluid. The hybrid nanofluids had augmented thermal conductivity compared to De-ionized water; however, the viscosity increased slightly.

2.3.2. Viscosity

The viscosity measurement of the nanofluids was conducted using the SV-10A Vibro-Viscometer, which was connected to a constant temperature bath. This measurement was carried out across a temperature range spanning from 20 °C to 50 °C. The instrument was calibrated through a one-point standard calibration procedure using pure water. Subsequently, the viscosity readings were collected for various volume fractions of the nanofluids and compared against those of De-ionized water. As depicted in Fig. 4, the results reveal a consistent decline in fluid viscosity as the temperature increases. And increase with the volume fraction. Notably, the γ-Al_2O_3-MWCNT/water nanofluids exhibited a slightly higher viscosity than De-ionized water. The nanofluid volume fraction of 0.3 vol% had a considerably higher viscosity than others due to more nanoparticles.

2.4. Experimental test stand

The test stand consists of the test section (constantly heated copper cylindrical block), centrifugal pump, ultrasonic flowmeter, collection tank, nozzle, heat exchanger, control valves, pulsating device {solenoid valves, diodes, function generator (TG120-20 MHz dial-set function generator) & power supply}, thermocouples, data acquisition systems and computer. A detailed description of the test rig is displayed in Fig. 5. The test section consists of a cylindrical copper block with a narrowed top surface diameter of 30 mm, insulated with PTFE on the sides and bottom. It is heated by six implanted cartridge heaters from the base of the copper block. Surface temperature is monitored using three K-type thermocouples inserted radially at about 3 mm close to the surface at different depths. The exiting cooling fluid temperature is estimated using five T-type thermocouples placed on a ring holder with a diameter of about 40 mm placed concentric to the top surface. The measured readings are logged using an Agilent datalogger and computer system. A single nozzle jet (D = 3 mm) was used throughout the experiment.

2.5. Test procedure

In this experimental work, the cooling of a flat-plate solar collector is simulated using the cylindrical copper block's flat-top surface. The instantaneous cooling of the flat-top surface of the copper cylinder, heated with constant heat flux and cooled with a pulsating nanofluid jet, will be analysed. The jet-cooling study was carried out in quasi-steady state conditions, and the performance of water and γ-Al_2O_3-MWCNT/water hybrid nanofluids (mixture of γ-Al_2O_3 and MWCNT of different particle size, with a particle mixing ratio of 60:40, of different volume concentration). Preceding each test, the collection tank is filled with seven and a half (7.5) liters of the nanofluid at ambient temperature. The thermal bathe linked with the double pipe heat exchanger is turned on and placed at 20 °C to stabilize the inlet temperature to an average of about 21 °C. The heater is turned on and allowed to supply constant heat flux to the copper block until an average temperature of about 80 °C. The pulsating device is turned on and set to the desired pulsating function. Afterwards, the fluid is pumped from the tank through the heat exchanger to the target surface at a set flow rate using an arrangement of bypass valve and control valve. The instantaneous fluid flow rate, the temperature of the surface and the exiting in the first 60 s are measured using the thermocouples, data-logger, and computer. The data is then retrieved from the computer and analysed.

2.6. Data reduction and uncertainty

2.6.1. Data reduction

The average pulsating Reynolds number (Re), Pulsating number (Pn), and Strouhal's number were calculated as follows. β is the pulsating duty cycle, which is the ratio of the pulsation flow-time to the overall pulsation cycle time.

$$\mathrm{Re} = \frac{\rho .\ U .\ D_{jet}}{\mu} \tag{1}$$

$$\mathrm{Pn} = \frac{\pi .\ F_{pul} .\ D_{jet}}{U} = \pi . Sr \tag{2}$$

$$\beta = \frac{Pulse - on\ \ time}{total\ cyle\ time} \times 100\% \tag{3}$$

The electrical power ($\dot{Q}_{\mathrm{elect}}$) supplied to the heater is estimated as the total heat flow introduced into the block. It is estimated on the target surface as heat flux considering the diameter of the target surface (D_t). The temperature of the target surface (top surface of the copper block) was measured using an approximation method, i.e., the weighted average heat flux method.

$$\dot{q}_{wt} = \frac{\sum_{i=1}^{4} (\Delta y \times \dot{q})_{i,i+1}}{\sum_{i=1}^{4} \Delta y_{i,i+1}} \tag{4}$$

$$T_{t,i} = T_{tc,i} - \frac{\dot{q}_{wt} \times \Delta x_{t,i}}{k_c} \tag{5}$$

$$T_t = \frac{\sum_{i=1}^{5} T_{t,i}}{5} \tag{6}$$

$$T_{exit} = \frac{\sum_{i=1}^{5} T_{e,i}}{5} \tag{7}$$

$$T_{bulk} = \frac{T_{inlet} + T_{exit}}{2} \tag{8}$$

Where T_{in} is the temperature of the fluid discharged from the nozzle, T_e is the average temperature of the fluid exiting the target surface after cooling, T_{bulk} is the bulk fluid temperature, T_t is the average temperature of the target surface, ΔT_{lm} is the log-mean temperature difference, $\dot{q}_{wt}$ is the weighted average heat flux, $\Delta y_{t,i}$ is the vertical distance between the different thermocouples point. The Nusselt number (Nu_{exp}) and the average Stanton number (St_m) was determined for datapoints where pulse-on occurred, while the pulse-off data where neglected.

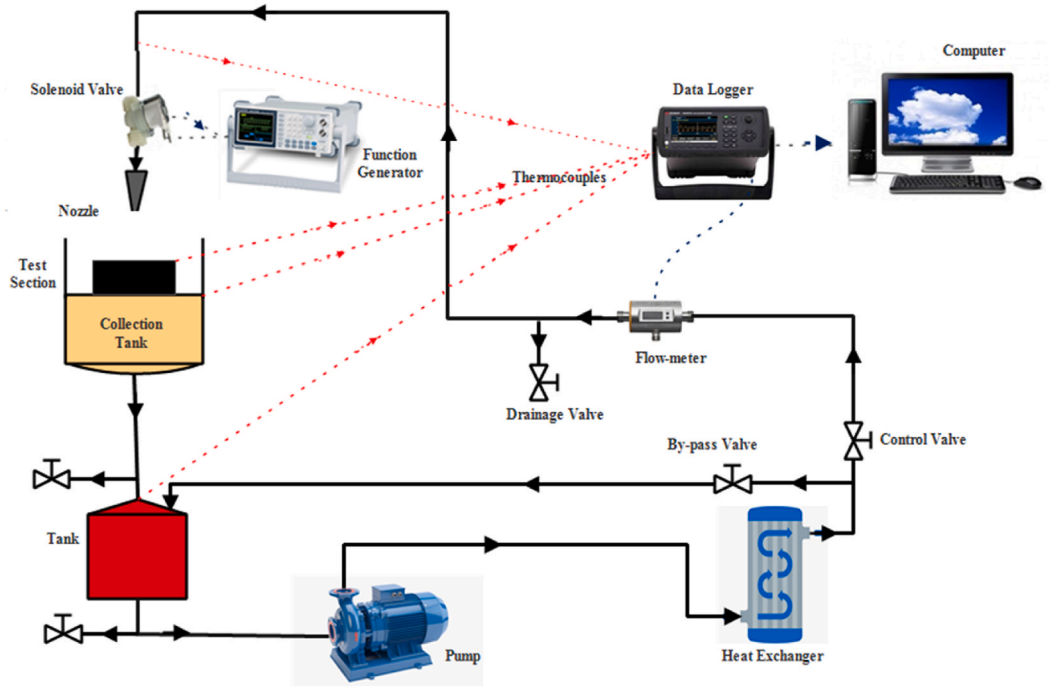

(a)

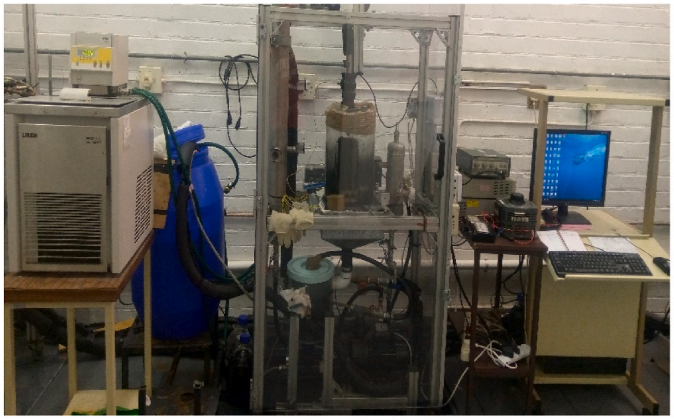

(b)

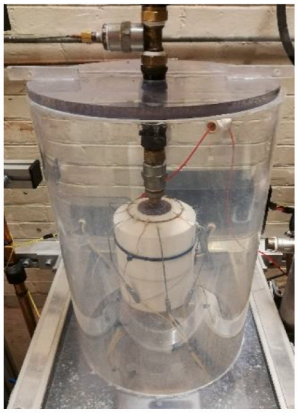

(c)

Fig. 5. Experimental test rig **(a)** Schematic View **(b)**Pictorial View **(c)** Test section.

$$Nu_{exp} = \frac{\dot{q}_{max} \times D_{jet}}{(\Delta T_{lm}).k} \quad 9$$

$$St_m = \frac{\dot{Q}_{elect}}{\dot{Q}_{max}} = \frac{\dot{Q}_{elect}}{\dot{m}c_p(T_e - T_{in})} \quad 10$$

2.6.2. Uncertainty analysis

The estimation of uncertainty in both measured and calculated parameters was conducted following the methodology outlined by Moffat [25] and Kline [26]. In the estimation of uncertainty (δx_i) in measuring a single parameter, it is crucial to ascertain both the bias (b) and precision (p) errors. The bias error signifies a constant error linked to the accuracy of the instrument, often provided by the instrument manufacturer. Conversely, the precision error is a stochastic or human-related error stemming from individual disparities, conditions, and the measurement's location. The uncertainty of a singular measurement and the overall uncertainty for each calculated parameter was determined using Equations (1) and (2) from the work of Kline. The entire analysis was executed utilizing a Python code's "Uncertainty" function, which computes the uncertainty within a 95 % confidence interval. A comprehensive summary of the uncertainty analysis can be found in Table 1.

Table 1
Uncertainty estimation of measured and calculated parameter.

Parameter	Maximum Uncertainty	Uncertainty value
Temperature	0.30 %	±0.1455 °C
delta T	0.74 %	±0.037 °C
Diameter	–	±0.01 mm
Area	0.067 %	±4.712 E−7 m^2
Q elect	1.62 %	±1.87 W
flowrate	0.72 %	±6.67 E−7 m^3/s
Reynold number	3.56 %	–
h	1.90 %	–
Nu	5.35 %	–

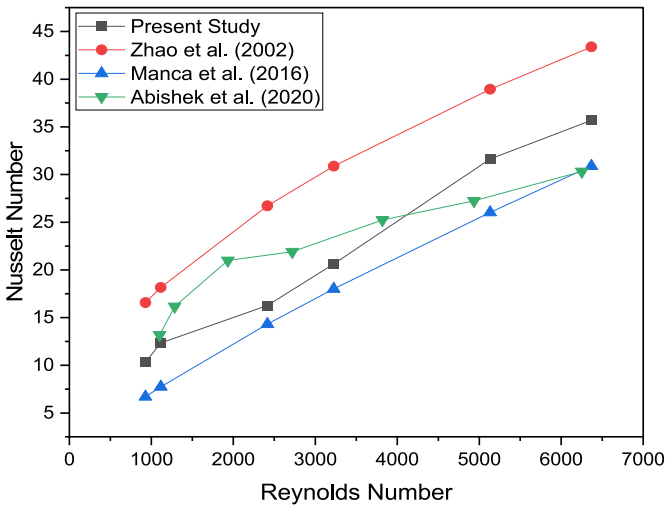

Fig. 6. Verification of experimental result with previous works on Continuous Jet Cooling.

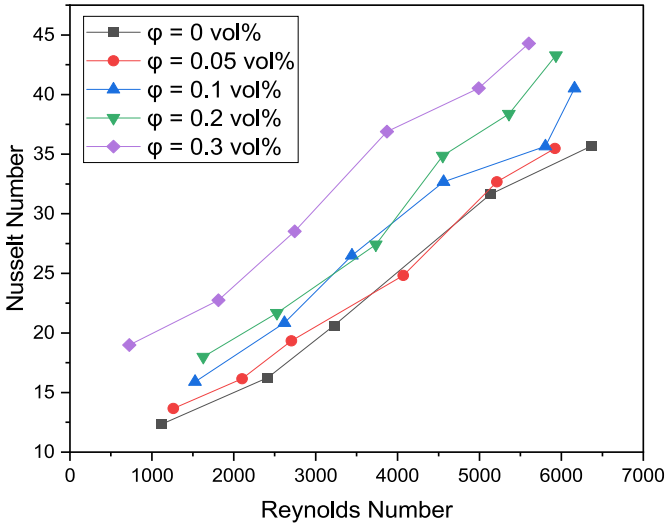

Fig. 7. Effect of Reynolds number on heat transfer.

$$\delta x_i = \left(b_i^2 + p_i^2\right)^{1/2} \quad (11)$$

$$\delta F = \left\{ \left(\frac{\delta F}{\delta x_1}\right)^2 \partial x_1 + \left(\frac{\delta F}{\delta x_2}\right)^2 \partial x_2 + \left(\frac{\delta F}{\delta x_3}\right)^2 \partial x_3 + \ldots + \left(\frac{\delta F}{\delta x_n}\right)^2 \partial x_n \right\}^{1/2} \quad (12)$$

3. Results and discussion

3.1. Verification of results

The test rig was initially validated to check the accuracy of its results with other previous studies using continuous jet impingement of water over a range of mass flow rates before testing with the hybrid nanofluid. The heat transfer performance result was compared to previous work by Zhao et al. [27], Manca et al. [28] and Abishek et al. [15]. Fig. 6., shows that the results had a close agreement with similar previous studies' outcomes in the considered flow condition.

3.2. Effect of Reynolds number & nanofluid volume fraction

The relationship between the Reynolds number and the Nusselt number was examined for a continuous jet impingement. It was observed that the Reynolds number is directly proportional to the Nusselt number as shown in Fig. 7. Also, It's evidence from the plot that the heat transfer increases with increasing nanoparticle concentration. An average heat transfer enhancement of 58.2 % was recorded for nanofluid. Volume fraction of 0.3 vol% when compared to De-ionized water in the same Reynold number range. Compared to other nanofluid volume fractions, the 0.3 vol% had better and distinct enhancement at all flow rates considered.

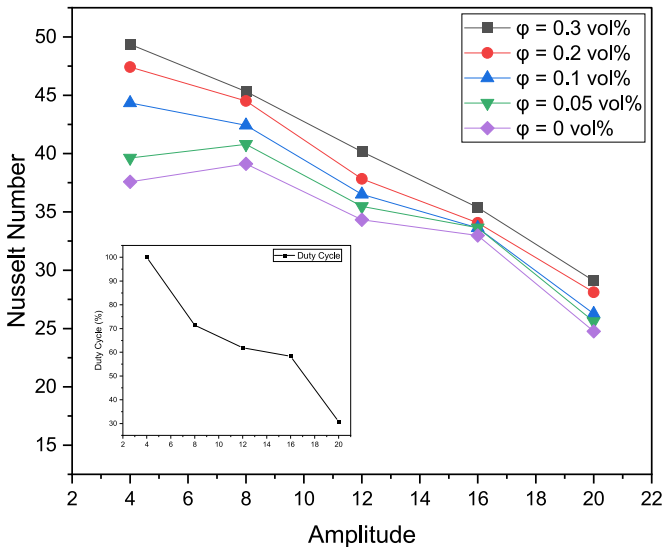

(a)

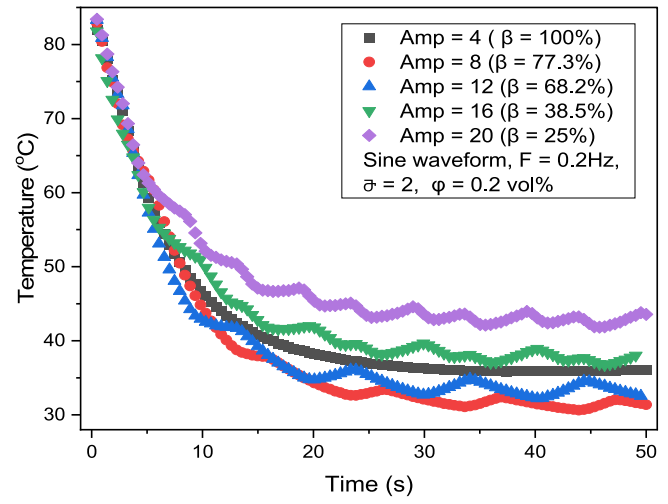

(b)

Fig. 8. (a) Impact of amplitude on heat transfer **(b)** Cooling curve at different amplitudes.

3.3. Effect of pulsating amplitude (A)

The pulsating amplitude is a significant factor that influences the hydrodynamic behavior of the pulsating jet impingement cooling system, which in turn affects the heat transfer performance. Studies by Mladin and Zumbrunnen [10], Behera et al. [12], Utturkar et al. [19], and Zhang et al. [20] have shown that pulsating jet impingement cooling has been reported to have augmented heat transfer than continuous jet impingement due to the continuous renewal of both the hydrodynamic

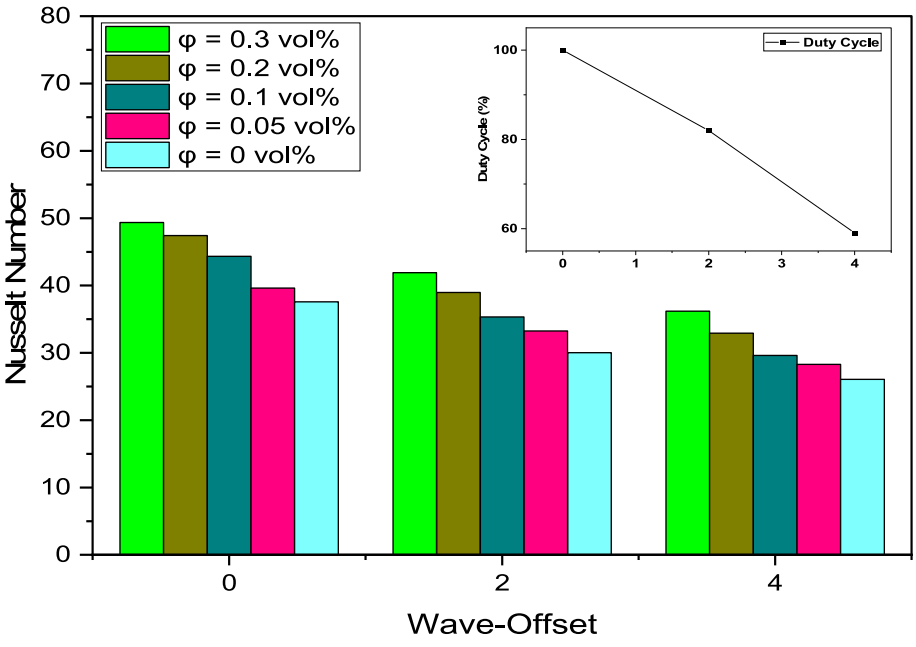

(a)

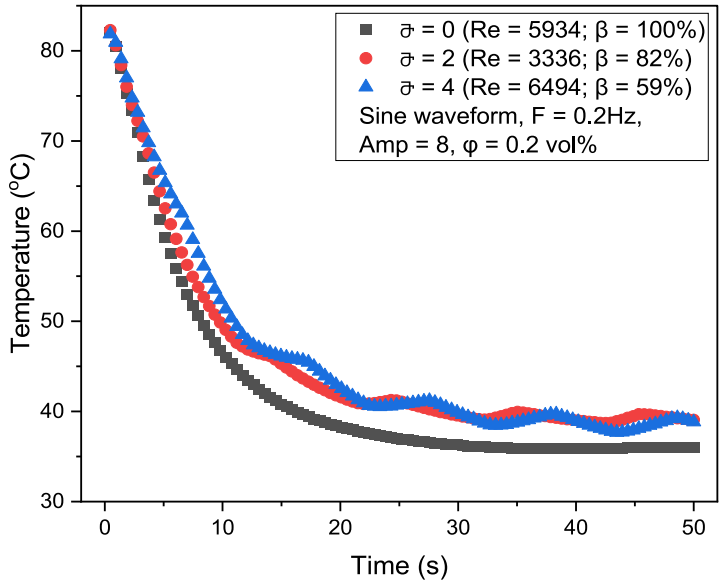

(b)

Fig. 9. (a) Impact of wave-offset on heat transfer **(b)** Cooling curve at different wave-offset.

and thermal boundary layer. Generally, most of their outcome shows that heat transfer efficiency for a pulsating jet increase with increasing amplitude and Strouhal number. The result obtained in this study considers the amplitude effect at a frequency (F = 0.2 Hz), wave offset (ϑ = 2), and a sine-waveform. The study outcome in Fig. 8(a) shows otherwise, as the convective heat transfer coefficient (*Nu*) reduced with increasing pulsating amplitude. This could be the condition explained by Mladin and Zumbrunnen, that large amplitude pulsation coupled with low frequency often led to reduced heat transfer. Notably, the pulsation was insignificant at a very low amplitude of 4 Vp, and the cooling behavior was the same as a continuous cooling jet. The distinguishing performance of the reduced nanofluid volume fraction was inversely proportional to the heat transfer rate. The duty cycle (β) shown in Fig. 8 (a) was found to be a function of the amplitude, as the value reduced with increasing amplitude. Fig. 8(b) shows the cooling curve for the different amplitude using the nanofluid volume fraction of 0.2 vol% as a case study. It shows that cooling at a pulsating amplitude of 8 Vp and 12 Vp had a better cooling rate that the "continuous" amplitude of 4 Vp, for a cooling time of 50 s. However, as the amplitude increases further, the cooling rate is reduced.

3.4. Effect of pulsating wave offset (ϑ)

The influence of wave-offset on the heat transfer performance of the different nanofluid volume fraction at a pulsating frequency (F = 0.2 Hz), amplitude (A = 8), and a sine-waveform was considered and presented in Fig. 9 (a) & (b). The experimental outcome in Fig. 9 (a) shows that the Nusselt number reduced with increasing wave offset. A similar trend can be seen for the duty cycle, indicating less pulse-on flow for each pulsating cycle as the wave offset increases. Fig. 9 (b) shows the

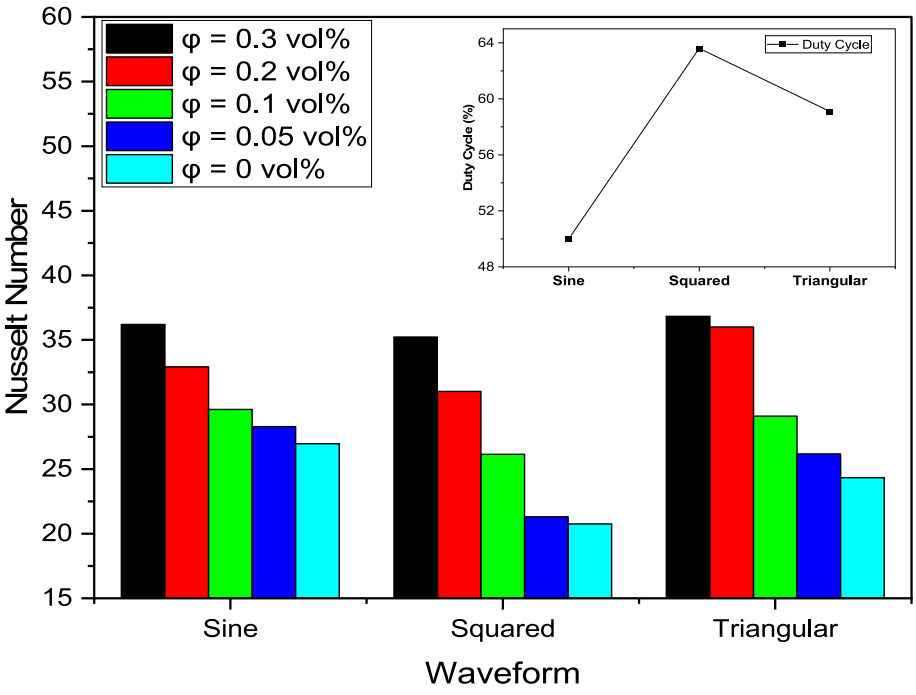

(a)

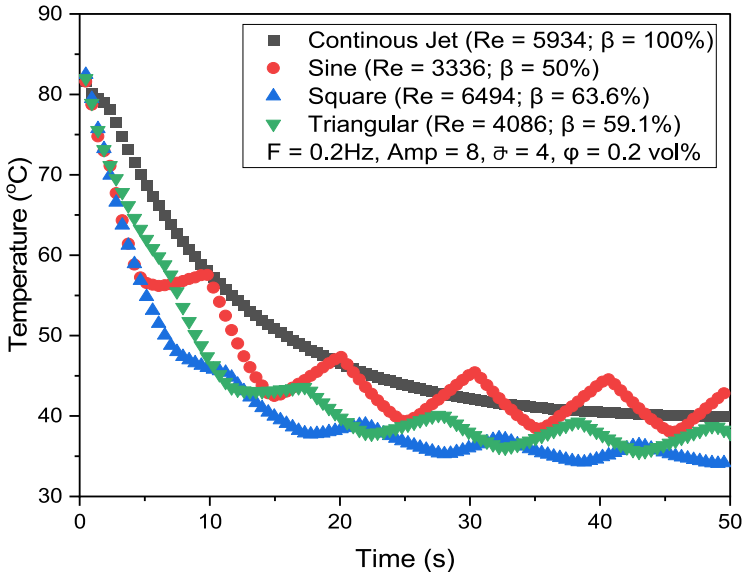

(b)

Fig. 10. (a) Influence of waveform on heat transfer **(b)** Cooling curve at different waveform.

cooling curve for different wave-offset. The cooling rate reduced slightly as the wave offsets increased. It is noteworthy to state that, for the wave-offset range ($0 < ∂ < 8$) available on the frequency generator used for this study, pulsating fluid flow was only possible for the range ($0 < ∂ < 4$). At a higher wave-offset ($∂ > 4$), the solenoid valve closes for longer, which could create unnecessary pressure in the system or damage the pump. Also, during pulsating cooling at high wave offset, the pulse-off time is longer, and the nanofluid might dry up on the surface, increasing the thermal boundary layer before the pulse-on. Hence, using an optimum wave offset for suitable heat transfer performance is advisable.

3.5. *Effect of pulsating waveform*

This study utilized three pulse generating waveforms (Sine, Square, Triangle) available on the function generator. The waveform's influence was insignificant, as shown in Fig. 10 (a). Although triangular waveform appeared to have peak duty cycle and heat transfer behavior, it has a limitation of varied offset. At offset ($∂ = 2$), pulsating frequency ($F = 0.2$) and amplitude ($A = 8$); the triangular and square waves had similar behavior to a continuous jet. However, the sine wave generally performs better for lower nanofluid volume fraction ($φ < 0.2$ vol%). The influence of the nanofluid volume fraction was clearly shown to increase the heat transfer rate significantly from the result. The cooling curve Fig. 10 (b) shows that all the waveforms had a better cooling rate than the

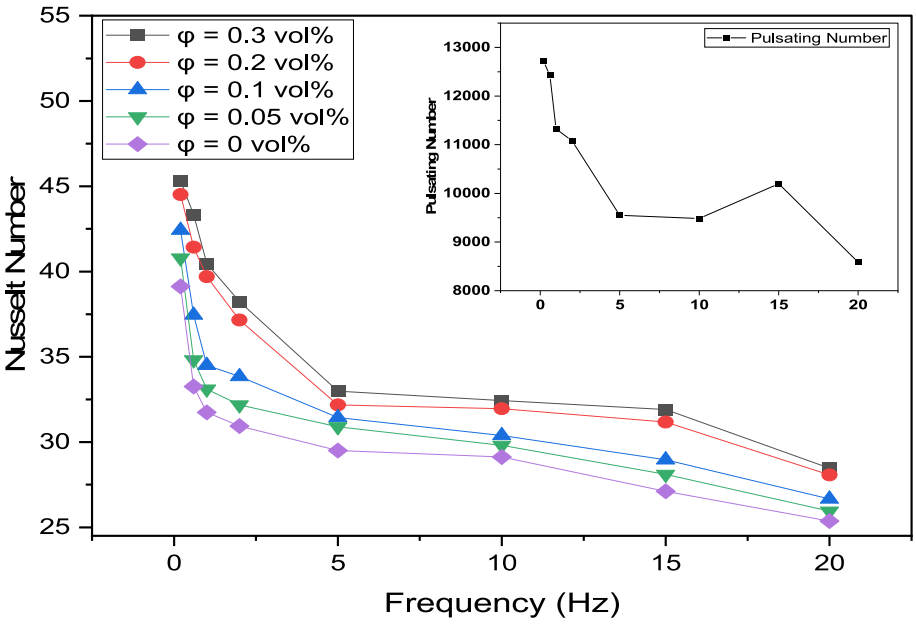

(a)

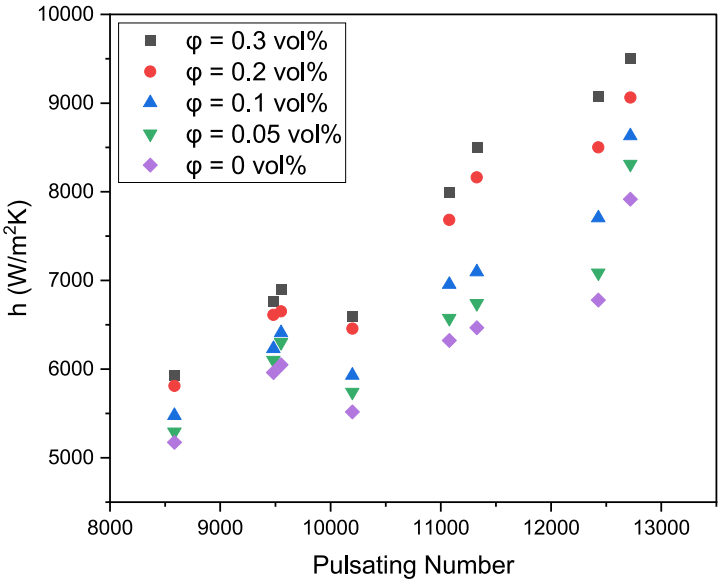

(b)

Fig. 11. Influence of **(a)** pulsating Frequency **(b)** pulsating number, on heat transfer.

continuous cooling jet, and the square waveform had a faster cooling rate compared to the other waveform.

3.6. *Effect of pulsating frequency*

Pulsating frequency is another significant factor extensively discussed in previous literature [13,17,29,30]. However, this study has been able to identify that the impact of frequency on the heat transfer at a low amplitude. The result shown in Fig. 11 (a) & (b) shows the cases of the de-ionized water and the hybrid nanofluid with volume fraction range (0.05 vol% $\leq \varphi \leq$ 0.3 vol%), amplitude (A = 8), wave-offset ($\bar{\sigma}$ = 2) and sine waveform. The study outcome establishes the relationship between pulsating frequency and heat transfer to be inversely proportional. This is because the duty cycle reduces with increasing frequency. Also, the plots show the relationship between the pulsating number, pulsating frequency, and the heat transfer coefficient. The pulsating number, which is a function of the fluid's average velocity and the pulsation duty cycle; appears to be a better parameter while defining the pulsating frequency. At higher duty cycles, longer pulse-on is observed, and higher average velocity is measured for a fixed mass flow rate. The graph Fig. 11 (a) & (b) shows that the pulsating number is inversely proportional to the frequency but directly related to the heat transfer coefficient. Generally, heat transfer enhancement increases with increasing pulsating numbers for all the fluids considered, and the

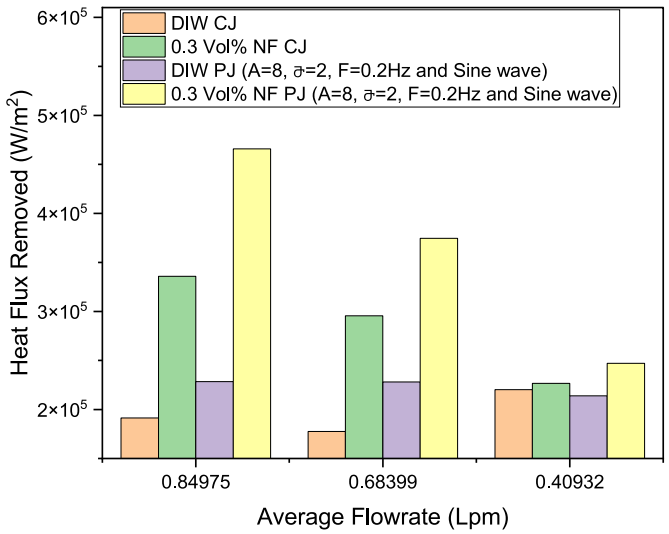

Fig. 12. Sequential Comparison of Cooling Performance of Continuous and Pulsating Jet Flow for De-ionized Water (DIW) and 0.3 vol% of the Hybrid Nanofluid.

highest volume fraction of nanofluids had the best heat transfer coefficient (h = 9508 W/m^{2}K).

3.7. Advances in pulsating jet cooling

The cooling performance while pulsating the cooling fluid was compared to corresponding continuous jet cooling under a fixed average fluid flow rate, as shown in Fig. 12. The result revealed that the pulsation jet had better heat transfer performance compared to the continuous jet. This is evidence for both D.I. water and the Al2O3-MWCNT/water hybrid nanofluid during continuous jet flow and pulsating jet flow. The heat flux removal rate increased by a factor of 1.43 while using pulsating hybrid nanofluid compared to continuous D.I water jet for cooling.

4. Conclusion

In this study, the extensive examination of continuous and pulsating jet impingement cooling using Al_2O_3-MWCNT/water nanofluid has unveiled key factors influencing heat transfer, including Reynolds number, nanofluid volume fraction, wave offset, pulsating frequency, and amplitude.

Optimized heat transfer performance was achieved with moderately high particle volume fractions (φ = 0.3 vol%), resulting in a substantial 24 % enhancement with a 0.3 vol% hybrid nanofluid under continuous jet impingement. Pulsating jet impingement exhibited a 20 % enhancement using a sine waveform (F = 0.2, A = 8, wave offset = 2). The impact of waveform on heat transfer proved negligible, with limited flexibility for certain waveforms.

For superior heat transfer, a high-duty cycle with low amplitude, low frequency, moderate wave offset, and the use of a sine waveform is recommended. These parameters play a pivotal role in achieving enhanced convective heat transfer characteristics.

The study's findings provide valuable insights for optimizing heat transfer in solar thermal collectors, guiding future design considerations and engineering decisions for efficient and environmentally sustainable cooling systems across various industrial applications.

The experimental outcomes complement numerical studies by Maatoug et al. [11], Selimefendigil & Oztop [21]. Lau et al. [22] and Mohammadpour et al. [23] address gaps in predicting the real behaviour of pulsating nanofluid jet impingement cooling.

In conclusion, this research contributes significantly to advancing knowledge in thermal sciences, offering practical implications for designing efficient cooling systems. Future endeavors could explore the scalability and feasibility of implementing pulsating nanofluid jet impingement cooling in real-world scenarios, propelling innovation in electronic devices, power electronics, data centers, and renewable energy systems.

Nomenclature

Re	Reynold number
Nu	Nusselt number
Pn	Pulsating number
Sr	Strouhal number
St	Stanton's number
T	Temperature
h	Heat transfer coefficient
k	Thermal conductivity
A	Amplitude
F	Frequency

CRediT authorship contribution statement

Emmanuel O. Atofarati: Data curation, Investigation, Software, Validation, Writing – original draft. **Mohsen Sharifpur:** Conceptualization, Funding acquisition, Methodology, Project administration, Resources, Supervision, Writing – review & editing. **Josua P. Meyer:** Funding acquisition, Methodology, Resources, Supervision, Writing – review & editing.

Declaration of competing interest

The authors declare that they have no known competing financial interests or personal relationships that could have appeared to influence the work reported in this paper.

Data availability

Data will be made available on request.

Acknowledgements

This research is a part of a project which was funded by the Technology Innovation Agency (TIA), an implementing entity of the RSA Department of Science and Technology which duly acknowledged and appreciated. The authors would like to appreciate all the kind assistance from the Department of Research & Innovation Support of the University of Pretoria.

Greek Characters

β	Duty cycle
∂	wave-offset
φ	Volume fraction
ρ	Density
γ	Gamma form

Abbreviations

Al_2O_3	Alumina oxide
MWCNT	Multi-Walled Carbon Nanotube
UV	Ultra-Violet
SDBS	Sodium DodecylBenzene Sulfonate
FEG-SEM	Field Emission Gun-Scanning Electron Microscope
TC	Thermal conductivity
DI	Di-ionized
CJ	Continuous Jet
PJ	Pulsating Jet
Vp	Voltage peak
Vol	Volume
PTFE	Polytetrafluoroethylene
$\dot{Q}_{elect}$	Electrical power
$\dot{Q}$	Quantity of heat
$\dot{q}$	Heat flux
I	Electric current
V	Electric voltage
D	Diameter
D_t	Target surface diameter
U	Velocity
$\dot{m}$	Mass flow rate
$\dot{V}$	Volumetric flow rate
A_{jet}	Cross-sectional area of Jet
T_{bulk}	Bulk temperature
Lpm	liters per minute

Subscripts and superscripts

i	initial
e	final
t	time
l	level
c	copper block
tc	Thermocouple
pul	pulsating

References

[1] E. Bergles, C.F. Ma, Boiling jet impingement cooling of simulated microelectronic chips, in: Heat Transfer in Electronic Equipment, 1983, pp. 5–12 [Online]. Available: https://ui.adsabs.harvard.edu/abs/1983htee.proc....5B/abstract. (Accessed 30 May 2023).

[2] F. Selimefendigil, H.F. Öztop, Jet impingement cooling and optimization study for a partly curved isothermal surface with CuO-water nanofluid, Int. Commun. Heat Mass Tran. 89 (Dec. 2017) 211–218, https://doi.org/10.1016/J.ICHEATMASSTRANSFER.2017.10.007.

[3] S. Abraham, R.P. Vedula, Distribution of effectiveness and Nusselt number over a corrugated surface impinged by a row of circular jets, IOP Conf. Ser. Mater. Sci. Eng. 1132 (1) (Apr. 2021) 012007, https://doi.org/10.1088/1757-899X/1132/1/012007.

[4] S.W. Chang, L.M. Su, Y. Zheng, Reciprocating impingement jet heat transfer with surface ribs, A J. Therm. Energy Gener. Transp. Storage, Convers. 13 (4) (Oct. 2010) 275–297, https://doi.org/10.1080/08916150050175462.

[5] J. Mohammadpour, F. Salehi, M. Sheikholeslami, M. Masoudi, A. Lee, Optimization of nanofluid heat transfer in a microchannel heat sink with multiple synthetic jets based on CFD-DPM and MLA, Int. J. Therm. Sci. 167 (Sep. 2021) 107008, https://doi.org/10.1016/J.IJTHERMALSCI.2021.107008.

[6] H.J. Carper, J.J. Saavedra, T. Suwanprateep, Liquid jet impingement cooling of a rotating disk, J. Heat Tran. 108 (3) (Aug. 1986) 540–546, https://doi.org/10.1115/1.3246968.

[7] T.W. Wei, et al., Experimental characterization and model validation of liquid jet impingement cooling using a high spatial resolution and programmable thermal test chip, Appl. Therm. Eng. 152 (Apr. 2019) 308–318, https://doi.org/10.1016/J.APPLTHERMALENG.2019.02.075.

[8] M. Forster, B. Weigand, Experimental and numerical investigation of jet impingement cooling onto a concave leading edge of a generic gas turbine blade, Int. J. Therm. Sci. 164 (Jun. 2021) 106862, https://doi.org/10.1016/J.IJTHERMALSCI.2021.106862.

[9] H. Deng, H. Li, J. Xu, Heat transfer in an impingement cooling channel under isothermal boundaries at high rotation numbers, Int. J. Heat Mass Tran. 182 (Jan. 2022) 121940, https://doi.org/10.1016/J.IJHEATMASSTRANSFER.2021.121940.

[10] A.V.S. Oliveira, et al., Experimental study of the heat transfer of single-jet impingement cooling onto a large heated plate near industrial conditions, Int. J. Heat Mass Tran. 184 (Mar. 2022) 121998, https://doi.org/10.1016/J.IJHEATMASSTRANSFER.2021.121998.

[11] S. Maatoug, et al., Pulsating multiple nano-jet impingement cooling system design by using different nanofluids for photovoltaic (PV) thermal management, Case Stud. Therm. Eng. 41 (Jan) (2023), https://doi.org/10.1016/J.CSITE.2022.102650.

[12] J. Mohammadpour, F. Salehi, M. Sheikholeslami, A. Lee, A computational study on nanofluid impingement jets in thermal management of photovoltaic panel, Renew. Energy 189 (Apr. 2022) 970–982, https://doi.org/10.1016/J.RENENE.2022.03.069.

[13] E.C. Mladin, D.A. Zumbrunnen, Alterations to coherent flow structures and heat transfer due to pulsations in an impinging air-jet, Int. J. Therm. Sci. 39 (2) (Feb. 2000) 236–248, https://doi.org/10.1016/S1290-0729(00)00242-8.

[14] Z. Trávníček, T. Vít, Impingement heat/mass transfer to hybrid synthetic jets and other reversible pulsating jets, Int. J. Heat Mass Tran. 85 (Jun. 2015) 473–487, https://doi.org/10.1016/J.IJHEATMASSTRANSFER.2015.01.125.

[15] S. Abishek, R. Narayanaswamy, Low frequency pulsating jet impingement boiling and single phase heat transfer, Int. J. Heat Mass Tran. 159 (Oct. 2020) 120052, https://doi.org/10.1016/J.IJHEATMASSTRANSFER.2020.120052.
[16] N. Neumann, A. Berthold, F. Haucke, D. Peitsch, P. Stathopoulos, Pulsed impingement turbine cooling and its effect on the efficiency of gas turbines with pressure gain combustion, J. Turbomach. 143 (7) (Jul. 2021), https://doi.org/10.1115/1.4050361/1101649.
[17] Z. Zhang, Q. Li, C. Bruecker, Q. Zhang, Enhanced thermal performance with high-amplitude intermittent impingement cooling, Int. J. Heat Mass Tran. 185 (Apr. 2022) 122359, https://doi.org/10.1016/J.IJHEATMASSTRANSFER.2021.122359.
[18] J. Wassenberg, P. Stephan, T. Gambaryan-Roisman, Heat transfer during pulsating liquid jet impingement onto a vertical wall, Heat Mass Transf. und Stoffuebertragung 57 (4) (Apr. 2021) 617–629, https://doi.org/10.1007/S00231-020-02973-Z/FIGURES/13.
[19] I. Sarkar, S. Chakraborty, J.M. Jha, S.K. Pal, S. Chakraborty, Ultrafast cooling of a hot steel plate using Cu-Al layered double hydroxide nanofluid jet, Int. J. Therm. Sci. 116 (Jun. 2017) 52–62, https://doi.org/10.1016/J.IJTHERMALSCI.2017.02.009.
[20] T. Wen, G. Zhu, L. Lu, Experimental and artificial neural network based study on the heat transfer and flow performance of ZnO-EG/water nanofluid in a mini-channel with serrated fins, Int. J. Therm. Sci. 170 (Dec. 2021) 107149, https://doi.org/10.1016/J.IJTHERMALSCI.2021.107149.
[21] F. Selimefendigil, H.F. Öztop, Identification of pulsating flow effects with CNT nanoparticles on the performance enhancements of thermoelectric generator (TEG) module in renewable energy applications, Renew. Energy 162 (Dec. 2020) 1076–1086, https://doi.org/10.1016/J.RENENE.2020.07.071.
[22] G.E. Lau, J. Mohammadpour, A. Lee, Cooling performance of an impinging synthetic jet in a microchannel with nanofluids: an Eulerian approach, Appl. Therm. Eng. 188 (Apr. 2021) 116624, https://doi.org/10.1016/J.APPLTHERMALENG.2021.116624.
[23] J. Mohammadpour, A. Lee, M. Mozafari, M.R. Zargarabadi, A.S. Mujumdar, Evaluation of Al2O3-Water nanofluid in a microchannel equipped with a synthetic jet using single-phase and Eulerian–Lagrangian models, Int. J. Therm. Sci. 161 (Mar. 2021) 106705, https://doi.org/10.1016/J.IJTHERMALSCI.2020.106705.
[24] S. Suseel Jai Krishnan, M. Momin, C. Nwaokocha, M. Sharifpur, J.P. Meyer, An empirical study on the persuasive particle size effects over the multi-physical properties of monophase MWCNT-Al2O3 hybridized nanofluids, J. Mol. Liq. 361 (Sep. 2022), https://doi.org/10.1016/j.molliq.2022.119668.
[25] R.J. Moffat, Describing the uncertainties in experimental results, Exp. Therm. Fluid Sci. 1 (1) (Jan. 1988) 3–17, https://doi.org/10.1016/0894-1777(88)90043-X.
[26] S.J. Kline, The purposes of uncertainty analysis, Trans. ASME 107 (1985) 154 [Online]. Available, https://scholar.googleusercontent.com/scholar?q=cache:uhRK987d1WQJ:scholar.google.com/+Kline+and+McClintock&hl=en&as_sdt=0,5. (Accessed 19 August 2023).
[27] Y. Zhao, T. Masuoka, T. Tsuruta, C.F. Ma, Conjugated heat transfer on a horizontal surface impinged by circular free-surface liquid jet, JSME Int. J. Ser. B Fluids Therm. Eng. 45 (2) (May 2002) 307–314, https://doi.org/10.1299/JSMEB.45.307.
[28] O. Manca, D. Ricci, S. Nardini, G. Di Lorenzo, Thermal and fluid dynamic behaviors of confined laminar impinging slot jets with nanofluids, Int. Commun. Heat Mass Tran. 70 (Jan. 2016) 15–26, https://doi.org/10.1016/j.icheatmasstransfer.2015.11.010.
[29] R.C. Behera, P. Dutta, K. Srinivasan, Numerical study of interrupted impinging jets for cooling of electronics, IEEE Trans. Compon. Packag. Technol. 30 (2) (Jun. 2007) 275–284, https://doi.org/10.1109/TCAPT.2007.898353.
[30] Y. Utturkar, M. Arik, C.E. Seeley, M. Gursoy, An experimental and computational heat transfer study of pulsating Jets, J. Heat Tran. 130 (6) (Jun. 2008), https://doi.org/10.1115/1.2891158/466852.